J Biomol NMR (2015) 61:299–310
DOI 10.1007/s10858-015-9903-1

ARTICLE

Lipid bilayer-bound conformation of an integral membrane beta barrel protein by multidimensional MAS NMR

Matthew T. Eddy · Yongchao Su · Robert Silvers · Loren Andreas · Lindsay Clark · Gerhard Wagner · Guido Pintacuda · Lyndon Emsley · Robert G. Griffin

Received: 30 October 2014 / Accepted: 20 January 2015 / Published online: 30 January 2015

Abstract The human voltage dependent anion channel 1 (VDAC) is a 32 kDa β-barrel integral membrane protein that controls the transport of ions across the outer mitochondrial membrane. Despite the determination of VDAC solution and diffraction structures, a structural basis for the mechanism of its function is not yet fully understood. Biophysical studies suggest VDAC requires a lipid bilayer to achieve full function, motivating the need for atomic resolution structural information of VDAC in a membrane environment. Here we report an essential step toward that goal: extensive assignments of backbone and side chain resonances for VDAC in DMPC lipid bilayers via magic angle spinning nuclear magnetic resonance (MAS NMR). VDAC reconstituted into DMPC lipid bilayers spontaneously forms two-dimensional lipid crystals, showing remarkable spectral resolution (0.5–0.3 ppm for ^{13}C line widths and <0.5 ppm ^{15}N line widths at 750 MHz). In addition to the benefits of working in a lipid bilayer, several distinct advantages are observed with the lipid crystalline preparation. First, the strong signals and sharp line widths facilitated extensive NMR resonance assignments for an integral membrane β-barrel protein in lipid bilayers by MAS NMR. Second, a large number of residues in loop regions were readily observed and assigned, which can be challenging in detergent-solubilized membrane proteins where loop regions are often not detected due to line broadening from conformational exchange. Third, complete backbone and side chain chemical shift assignments could be obtained for the first 25 residues, which comprise the functionally important N-terminus. The reported assignments allow us to compare predicted torsion angles for VDAC prepared in DMPC 2D lipid crystals, DMPC liposomes, and LDAO-solubilized samples to address the possible effects of the membrane mimetic environment on the conformation of the protein. Concluding, we discuss the strengths and weaknesses of the reported assignment

Matthew T. Eddy and Yongchao Su have contributed equally to this article.

Electronic supplementary material The online version of this article (doi:10.1007/s10858-015-9903-1) contains supplementary material, which is available to authorized users.

M. T. Eddy · Y. Su · R. Silvers · L. Andreas · L. Clark · R. G. Griffin
Department of Chemistry, Massachusetts Institute of Technology, Cambridge, MA 02139, USA

M. T. Eddy · Y. Su · R. Silvers · L. Andreas · L. Clark · R. G. Griffin (✉)
Francis Bitter Magnet Laboratory, Massachusetts Institute of Technology, Cambridge, MA 02139, USA
e-mail: rgg@mit.edu

Present Address:
M. T. Eddy
Department of Integrative Structural and Computational Biology, The Scripps Research Institute, La Jolla, CA 92037, USA

L. Andreas · G. Pintacuda · L. Emsley
Centre de RMN à Très Hauts Champs, Institut des Sciences Analytiques (CNRS, ENS Lyon, UCB Lyon 1), Université de Lyon, 69100 Villeurbanne, France

G. Wagner
Department of Biological Chemistry and Molecular Pharmacology, Harvard Medical School, Boston, MA, USA

approach and the great potential for even more complete assignment studies and de novo structure determination via ^{1}H detected MAS NMR.

Keywords VDAC · MAS · Recoupling · 2D lipid crystals

Introduction

High resolution structures of membrane-embedded proteins are of considerable interest for improving our understanding of fundamental biological processes and are essential for drug development. In recent years, the traditional methods of structure determination, solution nuclear magnetic resonance (NMR) spectroscopy (Reckel et al. 2011; Liang and Tamm 2007; Oxenoid and Chou 2005; Hwang et al. 2002; Fernández et al. 2001, 2004; Arora et al. 2001; Schnell and Chou 2008; Renault et al. 2009) and X-ray diffraction (Rosenbaum et al. 2007; Cherezov et al. 2007; Pryor et al. 2013; Hino et al. 2012; Brunner et al. 2014; Shimamura et al. 2011; Doré et al. 2011), have met with some success at determining de novo structures of membrane proteins. However, both methods are often applied to membrane proteins solubilized in detergent micelles and X-ray diffraction experiments are typically done at cryogenic temperatures. These conditions may detract from the biological relevance of the observed structures. Ideally, one would want to determine structures of membrane proteins in conditions that are as physiologically relevant as possible, i.e. in lipid bilayers that closely mimic the cellular membrane.

The challenge of structural biology studies in membrane bilayers is being addressed directly by solid state magic angle spinning NMR (MAS NMR) spectroscopy. Over the years, MAS NMR has elucidated details of membrane protein function including important studies of bacteriorhodopsin (Bajaj et al. 2009; Mak-Jurkauskas et al. 2008; Lansing et al. 2002; Griffiths et al. 2000a, b; Hu et al. 1998; Lakshmi et al. 1993; Thompson et al. 1992; Harbison et al. 1985; Ahuja et al. 2009), potassium channels (Bhate and McDermott 2012; Bhate et al. 2010; Schneider et al. 2008b; Ader et al. 2008; Lange et al. 2006), the acetyl choline receptor (Williamson et al. 1998, 2007; Krabben et al. 2009), and a large number of applications are described in several recent reviews (Eddy and Yu 2014; McDermott 2004, 2009; Cross et al. 2014; Hong et al. 2012). Membrane protein structures have been determined from approaches combining MAS NMR spectroscopy with X-ray diffraction (Tang et al. 2011), using oriented solid state NMR spectroscopy (Park et al. 2012), and with solution NMR spectroscopy (Verardi et al. 2011). De novo structures of relatively large membrane proteins and membrane protein complexes have been reported from restraints generated exclusively from MAS NMR spectroscopy (Wang et al. 2013). These studies pave the way for an improved understanding of the complex interactions between lipid bilayers and membrane protein structure and dynamics within a cellular context.

The first step in de novo NMR structure determination is the assignment process. This involves identifying individual resonances of backbone and side chain nuclei in multidimensional experiments, establishing correlations among observed signals, and associating connected resonances to specific amino acids from the protein sequence. As the assignment process requires relatively large amounts of homogeneous, isotopically labeled samples that yield high resolution spectra, sample preparation has often been the bottleneck in the assignment process and de novo structure determination of membrane proteins. Nevertheless, in recent years a number of groups have successfully prepared membrane protein samples of very high quality for MAS NMR spectroscopy and obtained partial or nearly complete assignments with a combination of selective isotopic labeling and multidimensional correlation experiments (Li et al. 2008; Frericks et al. 2006; Etzkorn et al. 2007; Zhou et al. 2012; Shi et al. 2009a, b, c; Higman et al. 2009; Hiller et al. 2005, 2008a; Andreas et al. 2010; Varga et al. 2007; Schneider et al. 2008a).

The human voltage dependent anion channel isoform 1 (referred to here as VDAC) is an integral membrane protein that is the main pathway of ion transport across the outer mitochondrial membrane (Mannella 1997; Hodge and Colombini 1997; Rostovtseva and Colombini 1996; Schein et al. 1976). Despite the huge progress of determining structures from solution NMR (Hiller et al. 2008b), X-ray diffraction data (Ujwal et al. 2008), and a combination of the two approaches (Bayrhuber et al. 2008) of the open state of VDAC, a structural explanation for the mechanism of gating between open and closed states remains elusive. Some studies have suggested a lipid bilayer environment may be required to observe full VDAC function (Shanmugavadivu et al. 2007); thus our efforts aim to delineate the influence of the surrounding bilayer on the structural properties of the channel.

Here we present the partial NMR assignments for VDAC samples reconstituted into lipid bilayers. Previously, we demonstrated that VDAC reconstituted into DMPC lipids could form highly homogeneous samples of two-dimensional lipid crystals that yielded spectra with good dispersion and narrow line widths of <0.5 ppm for both ^{13}C and ^{15}N nuclei at 750 MHz field strength (Eddy et al. 2012). Importantly, electrophysiological measurements performed on the same samples demonstrated that channels were functionally active and did not require the presence of cholesterol or detergents to properly gate (Eddy et al. 2012).

In the present study, a combination of two-dimensional and three-dimensional heteronuclear correlation experiments and selective isotopic labeling yielded assignments for 90 out of the 283 residues of the full length protein, including complete backbone and side chain assignments for the first 25 residues, which comprise the functionally important N-terminus. Nearly complete backbone chemical shift assignments of VDAC in detergent micelles have been reported, but so far assignments of VDAC in lipid bilayers are primarily limited to some of the residues among the first 20 of VDAC in lipid vesicles (Schneider et al. 2010). We compare our assignments with reported solution NMR chemical shifts as well as predicted torsion angles from the obtained resonance assignments, establishing the first steps toward detailed studies of the structure and dynamics of VDAC in lipid bilayers. Lastly, we also present preliminary ^{1}H detected ^{15}N–^{1}H heteronuclear correlation spectra of VDAC in lipid bilayers, illustrating the complementary and powerful technique of ^{1}H detection in MAS NMR experiments. Comparing solution NMR and solid-state NMR assignments, some potential advantages in the current MAS study are noted, including the detection and assignment of several loop regions, which are often difficult to assign in detergent solubilized membrane proteins due to line broadening from conformational exchange.

Experimental section

Materials

1,2-Dimyristoyl-*sn*-glycero-3-phosphocholine (DMPC) was obtained from Avanti Polar Lipids (Alabaster, AL). Octylpolyoxyethylene (octyl-POE) was obtained from Bachem (King of Prussia, PA). All other non-isotopically labeled reagents were obtained from Fisher. Isotopically labeled reagents used for VDAC expression were obtained from Cambridge Isotope Labs (Andover, MA).

Preparation of VDAC/DMPC 2D crystals

Protocols for expression, refolding, and purification of recombinantly expressed human VDAC were based on the work of Malia and Wagner (2007) and Hiller et al. (2008b). 2D crystals were prepared according to the procedures published in Eddy et al. (2012), modified from the protocol originally described by Dolder et al. (1999).

Isotopic labeling

To facilitate the process of unambiguous assignments, several isotopically labeled samples were prepared with complementary labeling schemes. In addition to a uniformly ^{13}C, ^{15}N labeled sample, several samples were prepared with various natural abundance amino acids added prior to protein expression. For example, WHIFY-VDAC was prepared by adding 1 mM each natural abundance Trp, His, Ile, Phe, and Tyr in addition to 2 g ^{13}C glucose and 1 g ^{15}N ammonium sulfate. Similarly FLY-VDAC was prepared by adding 1 mM each natural abundance Phe, Leu, and Tyr amino acids to a culture containing ^{13}C glucose and ^{15}N ammonium chloride. We refer to these samples as "reverse" labeled. In addition, several "forward" labeled samples were prepared by adding 1 mM ^{13}C, ^{15}N amino acids to media with natural abundance glucose and ammonium chloride. VPF-VDAC was prepared by addition of 1 mM ^{13}C, ^{15}N Val, Pro, and Phe, in addition to 1 mM natural abundance each of all other 17 amino acids and 2 g ^{12}C glucose and 1 g ^{14}N ammonium chloride. [U–^{2}H,^{15}N,^{13}C] VDAC was produced in media containing 99 % D_2O, 1 g $^{15}NH_4Cl$, and 3 g ^{13}C glucose. Protons were introduced at exchangeable sites during protein purification.

NMR spectroscopy

For all ^{13}C detected experiments, approximately 30 mg of two-dimensional lipid crystals (20 mg VDAC and 10 mg DMPC) were packed into Bruker 3.2 mM MAS rotors and sealed with epoxy to prevent sample dehydration. 1D spectra were acquired by using dipolar based cross polarization (CP) and INEPT (Morris and Freeman 1979) on an 800 MHz spectrometer at 20.0 kHz MAS and 283 K to investigate different spectral features of residues with different dynamics. 2D homonuclear ^{13}C–^{13}C correlation spectra were acquired with RFDR mixing at 12.5 kHz MAS and 750 MHz ^{1}H field strength on a custom built spectrometer (courtesy of Dr. D. Ruben) equipped with a 3.2 mM E-Free MAS probe (Bruker BioSpin, Billerica, MA) and at 20 kHz MAS and 900 MHz ^{1}H field strength on an Avance II spectrometer equipped with a 3.2 mM E-Free MAS probe (Bruker Biopsin, Billerica, MA). 83 kHz TPPM (Bennett et al. 1995) ^{1}H decoupling was used during evolution and acquisition periods (5.8 us pulse with relative phases of 0° and 13° spinning at 12.5 kHz and 0° and 18° spinning at 20 kHz). Each spectrum averaged 32 scans per point unless otherwise noted. 2D ^{15}N–^{13}C correlation spectra were acquired using ZF-TEDOR (Jaroniec et al. 2002b; Hing et al. 1993).

3D NCOCX and NCACX experiments were acquired using pulse sequences implementing scalar decoupling described by Ladizhansky and coworkers (Shi et al. 2008), SPECIFIC CP (Baldus et al. 1998) heteronuclear polarization transfer and DARR (TAKEGOSHI et al.

2001) [or RAD (Morcombe et al. 2004)] homonuclear polarization transfer at 12.5 kHz MAS and 16.667 kHz MAS frequencies and 750 or 900 MHz ^{1}H field strength, as noted in the text. For ^{1}H–^{15}N CP, a contact time of 1 ms was used with a constant r.f. field of 40 kHz applied on the ^{15}N channel and a 10 % linearly ramped r.f. field applied on ^{1}H matching the n = 1 Hartmann-Hahn condition. ^{15}N–^{13}C transfers implemented a contact time of 6 ms for ^{15}N–^{13}C$^{\alpha}$ and 8 ms for ^{15}N–^{13}C′ with 100 kHz ^{1}H CW decoupling. ^{13}C–^{13}C transfers were achieved either with 20 ms or 100 ms DARR mixing or ~5 ms RFDR mixing periods. Evolution and acquisition periods employed 83 kHz TPPM ^{1}H decoupling. Each 3D experiment was averaged for 16–24 scans per row. For each 3D experiment the time domain data matrix was 48 (t1) × 64 (t2) × 2048 (t3) with t1, t2, and t3 increments of 240, 160, and 11 µs, respectively for total evolution times of 11.5, 10.2, and 22.5 ms. The sample temperature was calibrated at a given spinning frequency with a specified amount of cooling gas and probe duty cycle by measuring the chemical shift of ^{79}Br as described previously (Thurber and Tycko 2009).

^{1}H detected 2D ^{15}N–^{1}H correlation spectra and 3D ^{13}C–^{15}N–^{1}H correlation spectra were recorded on approximately 2 mg of sample packed into a Bruker 1.3 mM rotor spinning at 60 kHz and at a proton frequency of 1 GHz. Optimal experimental conditions were applied according to Barbet-Massin et al.(Barbet-Massin et al. 2014) ^{1}H to ^{15}N CP applied a 1.5 ms contact time with a linear ramp on ^{1}H from 12 to 30 kHz on the ^{1}H channel and constant field of 38 kHz on the ^{15}N channel. For ^{15}N to ^{1}H CP prior to acquisition, 400 µs contact time was applied with a linear ^{1}H ramp from 29 to 11 kHz and constant field of 39 kHz on ^{15}N. Low power TPPM decoupling of 14 kHz was applied during indirect detection and WALTZ-16 decoupling of 10 kHz was applied during direct acquisition periods.

All data except 1D CP and INEPT analysis were processed in NMRPipe (Delaglio et al. 1995). 3D data sets were processed with 20 Hz Lorentzian line narrowing and 40 Hz Gaussian line broadening in the ^{15}N indirect dimension and 30 Hz Lorentzian line narrowing and 60 Hz Gaussian line broadening in the ^{13}C indirect and direct dimensions. Data were zero filled to 1,024 (t1) × 1,024 (t2) × 4,096 (t3) prior to Fourier Transformation. 3D data sets were then converted to Sparky files for the assignment process and preparation of figures (Goddard and Kneller). For displaying processed data in Sparky, the first contour level was cut at 4σ with each additional level multiplied by 1.2σ. 1D data sets were processed using the Bruker TopSpin 3.2 software package. Each spectrum was processed using the squared sine window function with an SSB of 3. Data was zero filled to 4,096 points prior to Fourier transformation.

Results

One- and two-dimensional spectroscopy and sample quality

We first acquired one-dimensional ^{13}C CP (Pines et al. 1973) and ^{13}C INEPT spectra to qualitatively probe for possible motion on very fast time scales, such as observed for regions of protein samples that have very long proton T_2 values, which are found for residues in very flexible regions including long C-termini or extensive loops (Etzkorn et al. 2007; Andronesi et al. 2005). Figure 1 compares a representative 1D ^{13}C CP experiment (A) and 1D ^{13}C INEPT spectra (B and C) obtained on uniformly labeled VDAC in DMPC. Taking the number of scans into account, the INEPT signals are much weaker than the dipolar based CP intensity, indicating that no very fast motion was observed; thus VDAC's C and N termini and

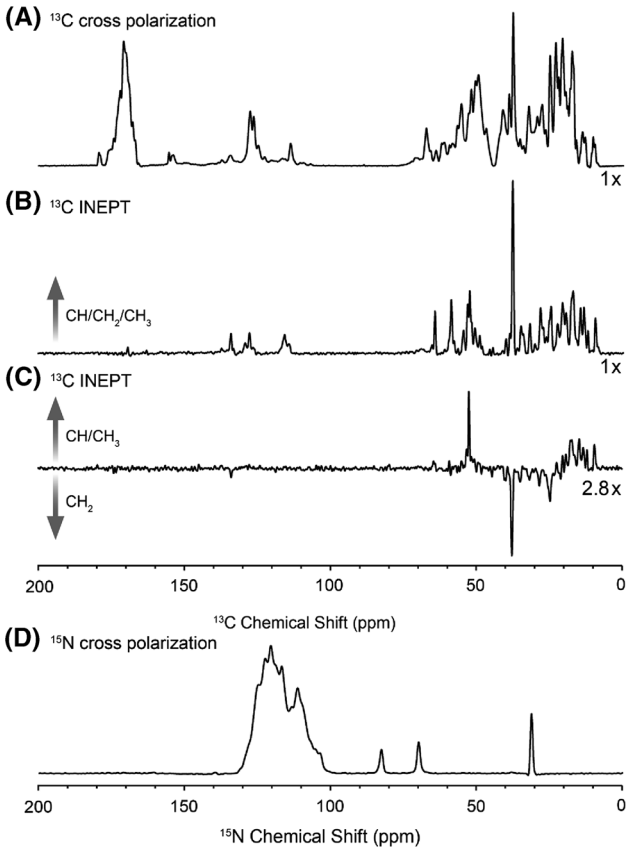

Fig. 1 One-dimensional ^{13}C and ^{15}N cross polarization (**a**, **d**) and INEPT (**b**, **c**) spectra of U–^{13}C,^{15}N VDAC1 in 2D DMPC lipid crystals at 800 MHz field strength and 20.0 kHz spinning frequency at 283 K. The ^{13}C CP spectrum was obtained with 256 scans, the ^{15}N CP spectrum was obtained with 1,024 scans, and the INEPT spectra were obtained with 4,096 and 1,024 scans for B and C, respectively. As a visual aid, the spectrum in **c** was scaled by a factor of 2.8 relative to the spectra in (**a**, **b**)

loop regions must not be very dynamic in our lipid bilayer preparation. Some of the sharp signals in the ^{13}C CP aliphatic region were tentatively assigned to the acyl chains of the DMPC lipids.

Two-dimensional ^{13}C–^{13}C experiments demonstrated that VDAC reconstituted into DMPC formed very homogenous samples that yielded exceptionally narrow line widths (0.5–0.3 ppm ^{13}C and <0.5 ppm ^{15}N at 750 MHz) for uniformly labeled samples of the nearly 300-residue protein, consistent with our previously reported results (Eddy et al. 2012).

To establish a starting point for assignments, we prepared several specifically labeled samples where ^{13}C, ^{15}N labeled amino acids were added to M9 minimal media and all other amino acids were added unlabeled at a final concentration of 1 mM. The addition of 1 mM unlabeled amino acids minimized scrambling, and a second sample prepared without the unlabeled amino acids showed significantly more peaks that were not from Val, Pro, or Phe residues (data not shown).

One combination where this worked well was with a sample prepared from ^{13}C, ^{15}N Val, Pro, and Phe. 2D ^{13}C–^{13}C and ^{15}N–^{13}C correlation spectra of VPF-VDAC are shown in Fig. 2. One-bond intraresidue ^{13}C–^{13}C contacts were obtained with radio frequency-driving recoupling (RFDR) (Bennett et al. 1998) using a short mixing period and one-bond intra- and inter-residue ^{15}N–^{13}C contacts were obtained with ZF-TEDOR (Hing et al. 1993; Jaroniec et al. 2002a) optimized with a short mixing period. These spectra permitted identification of sequentially labeled residues. Because of the relatively low occurrences of pairs of V, P, and F residues, we could immediately identify ^{15}N–^{13}CO contacts for the segment V3-P4-P5 from the N-terminal region. These assignments were confirmed from long-range inter-residue contacts identified in experiments employing long PDSD mixing (200–300 ms). The favorable spectral dispersion and number of peaks with unique chemical shifts permitted assignment of several additional residues. These early assignments provided anchor points for subsequent assignments from more complex 2D and 3D data sets. The sample also helped to validate assignments obtained from three-dimensional experiments on uniformly labeled VDAC (vide infra).

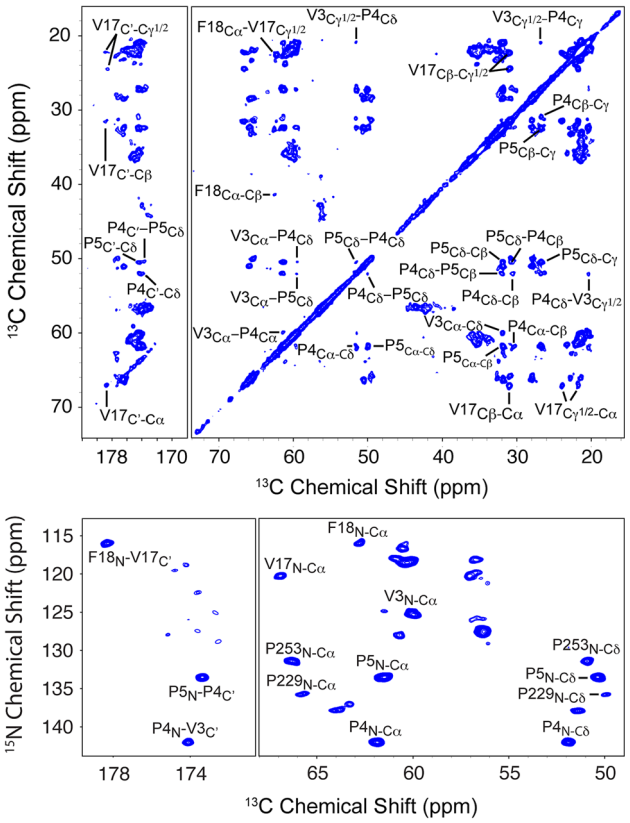

Fig. 2 2D correlation spectra and assignments of ^{13}C,^{15}N VPF labeled VDAC. *Top* ^{13}C–^{13}C correlation spectrum obtained with 200 ms PDSD mixing. A number of intra- and inter-residue contacts were identified and used for assignment starting points. *Bottom* ^{13}C–^{15}N TEDOR correlation spectrum optimized for one-bond intra- and inter-residue contacts. The PDSD and TEDOR experiments averaged 192 and 256 scans, respectively, over total experiment times of 120 and 96 h. The temperature was maintained at 278 K for both experiments

Three-dimensional spectroscopy, resonance assignment strategy, and isotopic labeling approaches

The overlap of signals from different amino acids can impede resonance assignment significantly, particularly in larger proteins. To address this problem, several groups have reported on the benefit of so called reverse isotopic labeling (Shi et al. 2009a; Etzkorn et al. 2007; Heise et al. 2005), where certain unlabeled amino acids are added to *E. coli* growth media in the presence of uniformly labeled glucose. The resulting sample, in principle, is uniformly labeled except for the selected amino acids. In our experience, the amino acids Trp, His, Ile, Phe, Leu, and Tyr appeared to provide the most specific labeling with minimal to no scrambling of ^{13}C labels, consistent with previously reports (Shi et al. 2009a). We prepared several complementary labeled samples: U–^{13}C,^{15}N–[^{12}C,^{14}N]-FLY-VDAC (FLY-reverse labeled), and [^{12}C,^{14}N]-WHIFY-VDAC (WHIFY-reverse labeled). Example ^{13}C–^{13}C RFDR correlation spectra of all three samples are shown in Fig. 3, with expansions of ^{13}C–^{13}C aliphatic regions shown in the middle and right panels highlighting the simplified spectra observed with reverse labeling. We attempted to prepare samples with reverse labeling of Ala, Ser Thr, and Gly, but these showed significant signals from the residues that were intended to be unlabeled and also showed a complex labeling pattern for other residue types.

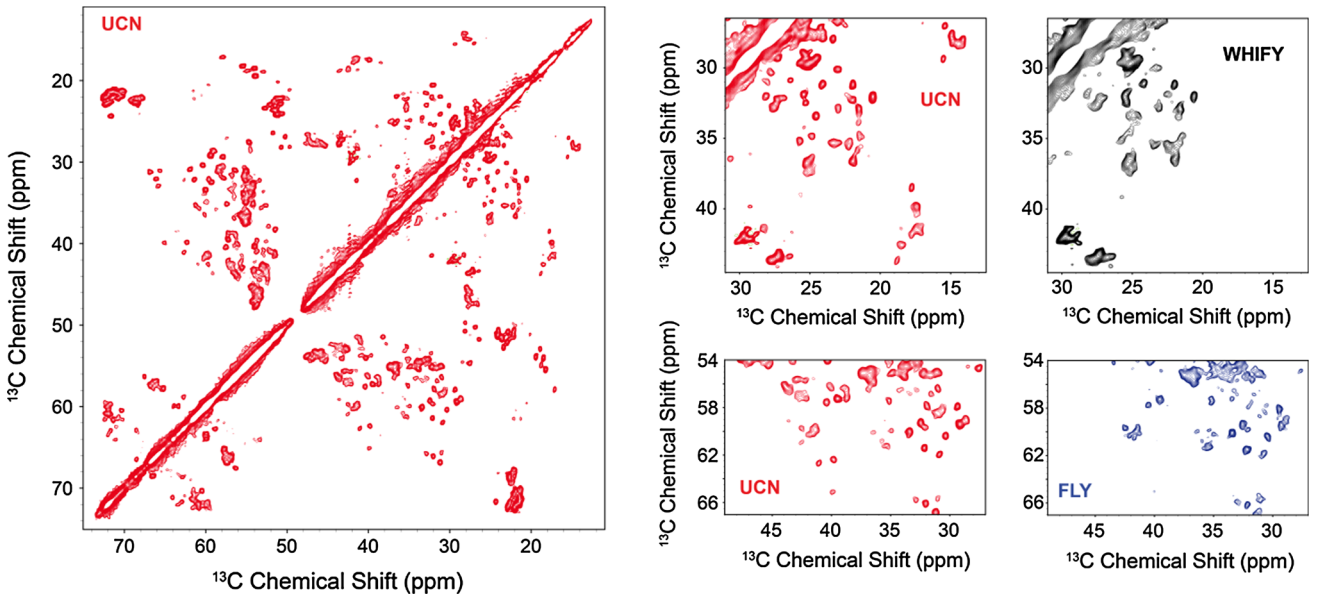

Fig. 3 2D ^{13}C–^{13}C RFDR correlation spectra of U–^{13}C,^{15}N-VDAC (*red*), FLY-reverse labeled VDAC (*blue*), and WHIFY-reverse labeled VDAC (*black*). All spectra were acquired at 750 MHz ^{1}H field strength, 12.5 kHz MAS frequency, with 1.3 ms RFDR mixing and 83 kHz TPPM ^{1}H decoupling during evolution and acquisition periods. The *middle* and *right panels* are expansions of the full aliphatic–aliphatic spectra for the same regions with each labeling scheme. Each experiment averaged 32 scans with a total acquisition time of approximately 24 h per experiment. The temperature was maintained at 278 K for each experiment

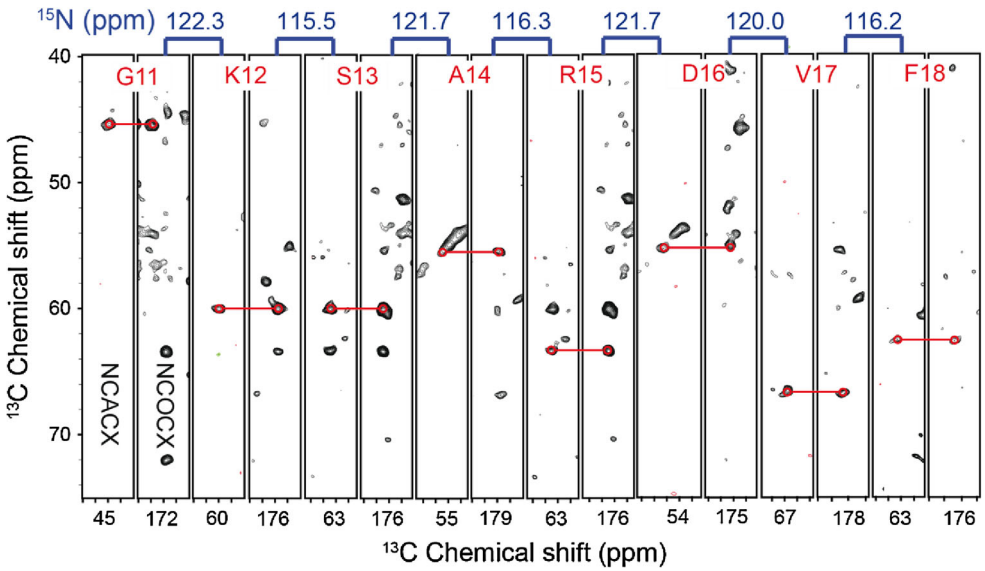

Fig. 4 Example strip plots of alternating NCACX and NCOCX spectra showing sequential backbone assignment for residues 11 through 18. Each experiment averaged 16 scans and took 7 days to acquire. The sample temperature was maintained at 278 K

Although the resolution and dispersion in ^{13}C–^{13}C 2D correlation experiments are exceptionally good, reliable, unambiguous assignments could not be obtained from 2D spectra alone, even with selectively forward or reverse labeled samples. The reason for this is the significant spectral crowding in 2D heteronuclear ^{15}N–^{13}C spectra and in the CO-aliphatic regions of 2D homonuclear correlation spectra that are needed for establishing unambiguous backbone correlations. To overcome this issue, we measured three-dimensional heteronuclear experiments on uniformly and selectively labeled VDAC. 3D-NCACX experiments established intraresidue correlations and 3D-NCOCX experiments established interresidue correlations between residue i and residue i−1. We obtained unambiguous assignments by combining 3D-NCACX and 3D-NCOCX spectra with resolved signals from the aliphatic–aliphatic regions of 2D ^{13}C homonuclear correlation experiments. 2D strips from 3D correlation experiments are shown in Fig. 4, illustrating a typical backbone walk from residues 11 to 18. The most useful experiments were on

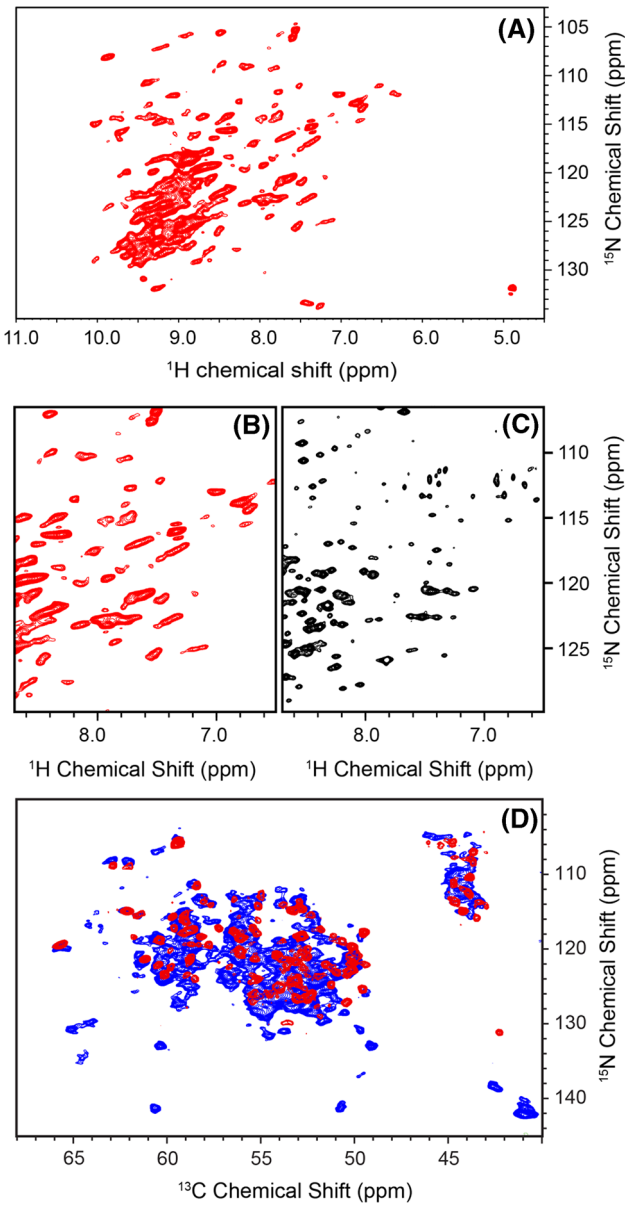

Fig. 5 **a** ^{1}H detected ^{15}N–^{1}H correlation spectra of VDAC in DMPC 2D lipid crystals recorded at 1 GHz ^{1}H field strength and $\omega_r/2\pi = 60$ kHz. *Bottom panels* compare ^{1}H detected MAS spectra of VDAC in DMPC 2D lipid crystals **b** with the same region of a ^{1}H–^{15}N-TROSY experiment of VDAC in LDAO detergent micelles (**c**). The solution NMR spectrum in **c** is reproduced from Hiller et al. (2010). **d** Comparison of a 2D ^{15}N–^{13}C TEDOR spectrum of [U–^{1}H,^{13}C,^{15}N]-VDAC sample (*blue*) and 2D ^{15}N–^{13}C projection from a 3D ^{13}C–^{15}N–^{1}H spectrum of [U–^{2}H,^{13}C,^{15}N]VDAC (*red*)

uniformly labeled samples obtained with relatively short DARR mixing for predominantly one-bond carbon–carbon transfers, and also longer DARR mixing to obtain more extensive contacts among side chain resonances (Fig. 4).

We also prepared samples using 1,3–^{13}C or 2–^{13}C glycerol as carbon sources. The resulting labeling scheme has been well characterized and is known to produce a checkerboard or alternating pattern (Higman et al. 2009). While this labeling did improve ^{13}C line widths, especially for C$^{\alpha}$ sites, low fractional labeling of the side chains resulted in significant loss of relayed polarization and ultimately low signal intensities were observed. Low intensities or missing peaks for some residues were also noted in uniformly labeled samples, possibly due to dynamics interferring with polarization transfer or decoupling. The situation was exacerbated for the glycerol labeled sample. Due to the low signal-to-noise in 3D spectra we chose not to include it in the current analysis in order to report the most reliable assignments possible.

Summary of assignments and assignment table

Based on analysis of two-dimensional and three-dimensional correlation experiments, we were able to assign 90 residues or 327 ^{13}C and ^{15}N atoms from the VDAC sequence. The complete assignment table has been deposited in the BMRB (accession number: 25413) can found in the Supporting Information.

Preliminary ^{1}H detected experiments

^{1}H-detection in MAS NMR has emerged as an important technique providing improved sensitivity and spectral resolution. Figure 5a, b shows ^{15}N–^{1}H correlation spectra of VDAC in DMPC bilayers. A comparison with a ^{1}H–^{15}N-TROSY spectrum of VDAC in LDAO micelles acquired by solution NMR spectroscopy is shown in Fig. 5c. Comparable resolution between the two spectra are observed. Additionally, Fig. 5d shows an overlay of a 2D ^{15}N–^{13}C projection from an ^{1}H-detected 3D hNCA experiment and ^{13}C detected ^{15}N–^{13}C TEDOR spectrum. The 2D plane from the ^{1}H detected 3D experiment is well-resolved and shows a nearly identical pattern of peaks compared with the TEDOR spectrum; peaks located between 130 and 145 ppm in the ^{15}N dimension are mostly prolines and not detected in the ^{1}H experiment, as expected. These representative 2D spectra exhibit excellent resolution that will facilitate the complete assignment of this 283-residue protein in lipid bilayers by MAS NMR, and preliminary analysis indicates that additional residues are observed in the ^{1}H-detected spectrum over conventional ^{13}C-detected experiments.

Discussion

Secondary structure analysis and comparison with detergent micelle and DMPC liposome preparations

To obtain information on the secondary structure of the assigned VDAC residues, we inputted chemical shifts for

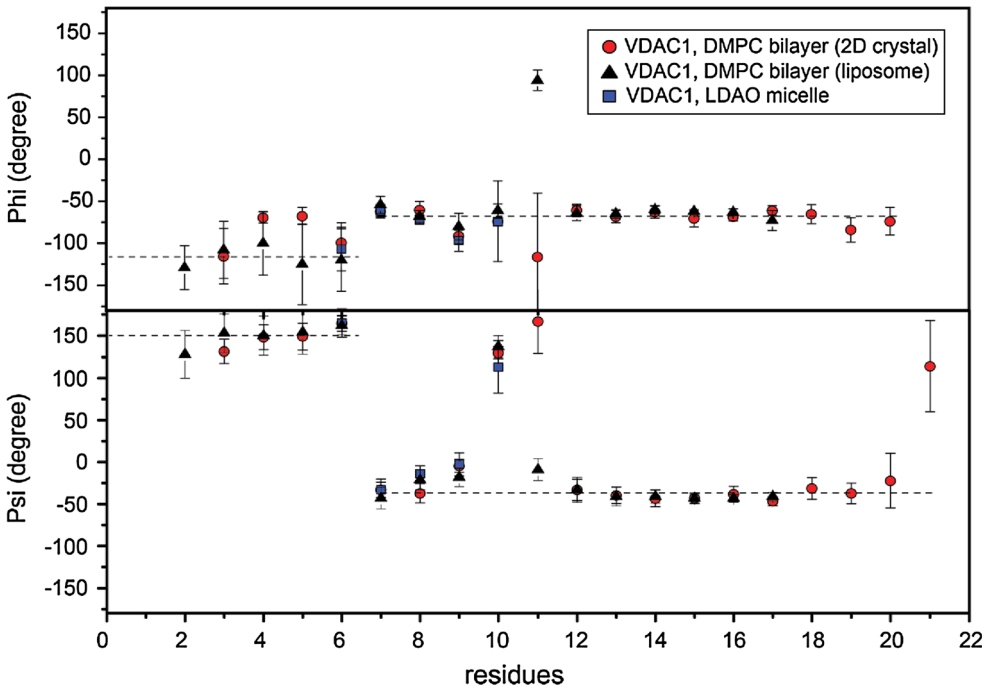

Fig. 6 Comparison of predicted torsion angles of residue 1–22 for VDAC reconstituted into DMPC 2D lipid crystals (*red circles*, data of current study), DMPC liposomes [*black triangles*, (Schneider et al. 2010)], and LDAO micelles [*blue squares*, (Hiller et al. 2008b)]. Torsion angles were empirically predicted using TALOS+

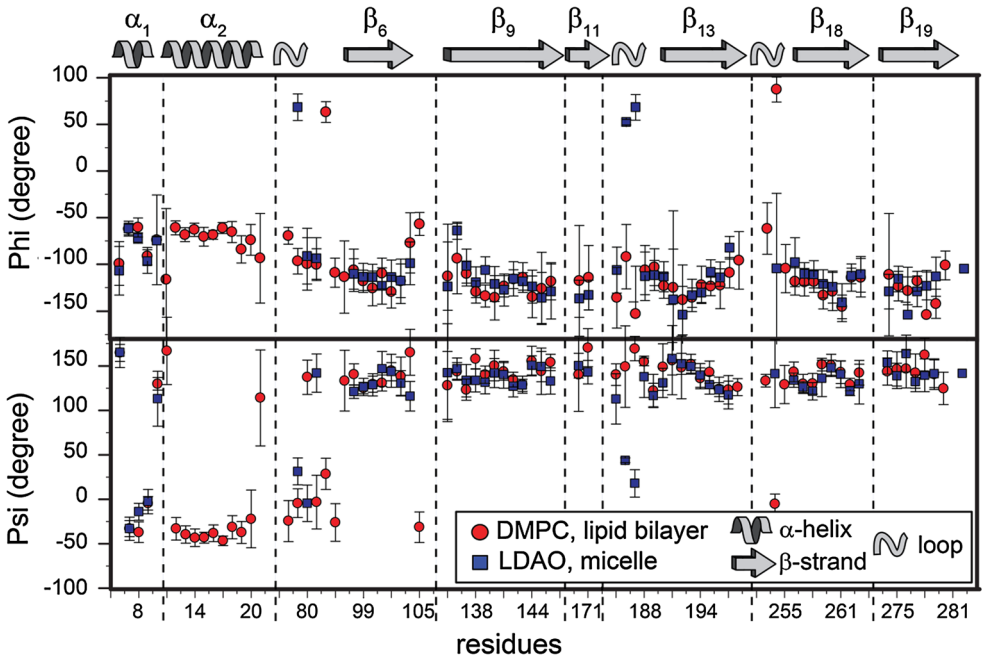

Fig. 7 Plot of the TALOS+ predicted torsion angles of VDAC in DMPC lipid bilayers from the present study and predicted torsion angles from the published chemical shifts for VDAC solubilized in LDAO detergent micelles (Hiller et al. 2008b). Secondary structure types are indicated at the *top* and in the figure legend

assigned C^{α}, C^{β}, CO, and N backbone residues into the program TALOS+, which empirically predicts phi and psi torsion angles (Shen et al. 2009). This allowed us to analyze the predicted secondary structure for VDAC in DMPC 2D lipid crystals for the entire N-terminus and a number of beta strands and loop regions.

VDAC's N-terminus has been observed to be critical for channel gating and important in various cellular functions. We were first interested to see how the secondary structure of this region compared for VDAC preparations in different lipid or micelle environments. To compare predicted secondary structures for VDAC in LDAO micelles and DMPC liposomes we inputted the chemical shift assignments of VDAC in DMPC liposomes (Schneider et al. 2010) for residues 2 through 17, and the chemical shifts for residues 6–10 from Hiller et al. (Hiller et al. 2008b). A comparison

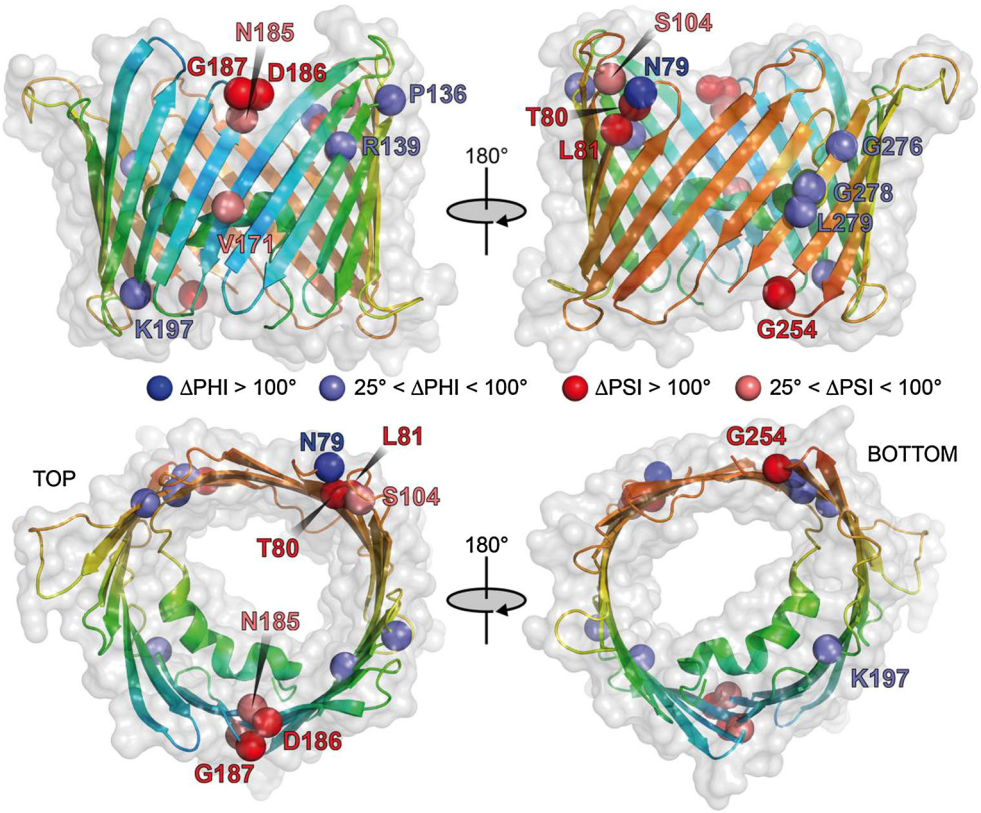

Fig. 8 3D structure of VDAC illustrating medium and large differences in predicted torsion angles between VDAC in LDAO micelles and DMPC 2D lipid crystals. Residues showing differences are shown as *spheres*. Large differences in PHI and PSI angles (larger than 100°) are shown in *dark blue* or *dark red*, respectively. Medium differences in PHI and PSI angles (between 25° and 100°) are shown in *light blue* or *light red*, respectively. Structures were generated from PDB ID 3EMN using the Pymol software package

of all three sets of predicted torsion angles for the first 22 residues is shown in Fig. 6. Overall, there is good agreement among the three sets of predicted torsion angles, showing similar secondary structure predicted. The largest difference appears for residue G11. However, glycine appears not to be a sensitive reporter of protein conformation due to its lack of the Cb site, which is an important determinant for the dihedral angle calculation via TALOS.

Next we compared secondary structure predictions for assigned residues beyond the N-terminus for VDAC in 2D lipid crystals and VDAC in LDAO micelles. As with the comparison of N-terminal residues, assignments of VDAC in LDAO were taken from Hiller et al. Again we used TALOS+ to predict the secondary structure using N, C^{α}, C^{β}, and CO chemical shifts. Figure 7 shows a plot comparing the two sets of TALOS+ predicted secondary structures.

Overall, the predicted backbone torsion angles between VDAC in LDAO and in 2D DMPC lipid crystals appear similar. However, some residues show significant differences in torsion angles. All residues showing large differences (larger than 100°) are located at loop regions of the membrane protein. Furthermore, six out of ten residues showing medium differences (between 25° and 100°) are located at loop regions as well. These residues are located near the interface between the membrane-spanning region and solvent accessible region of VDAC, illustrated in Fig. 8. Differences in predicted torsion angles for these regions could arise from different interactions between VDAC and LDAO or DMPC lipid bilayers, or another explanation could be the presence of protein–protein contacts between layers in the 2D crystals.

Based on our preliminary assignments and secondary structure analysis, the outlook for de novo structure determination of beta barrel membrane proteins with solid state NMR spectroscopy is very promising. It is worth noting that for many beta barrel membrane proteins, loop regions are often unobserved because of line broadening due to conformational exchange in detergent micelles. Thus MAS NMR may have a distinct advantage, not only offering structure determination of membrane proteins in lipid bilayers but in principle more complete assignments may be obtained.

Acknowledgments This research was supported by NIH Grants EB001960 and EB002026.

References

Ader C, Schneider R, Hornig S, Velisetty P, Wilson EM, Lange A, Giller K, Ohmert I, Martin-Eauclaire M-F, Trauner D, Becker S,

Pongs O, Baldus M (2008) A structural link between inactivation and block of a K+ channel. Nat Struct Mol Biol 15(6):605–612

Ahuja S, Hornak V, Yan ECY, Syrett N, Goncalves JA, Hirshfeld A, Ziliox M, Sakmar TP, Sheves M, Reeves PJ, Smith SO, Eilers M (2009) Helix movement is coupled to displacement of the second extracellular loop in rhodopsin activation. Nat Struct Mol Biol 16(2):168–175

Andreas LB, Eddy MT, Pielak RM, Chou J, Griffin RG (2010) Magic angle spinning NMR investigation of influenza A M2(18–60): support for an allosteric mechanism of inhibition. J Am Chem Soc 132(32):10958–10960

Andronesi OC, Becker S, Seidel K, Heise H, Young HS, Baldus M (2005) Determination of membrane protein structure and dynamics by magic-angle-spinning solid-state NMR spectroscopy. J Am Chem Soc 127(37):12965–12974

Arora A, Abildgaard F, Bushweller JH, Tamm LK (2001) Structure of outer membrane protein. A transmembrane domain by NMR spectroscopy. Nat Struct Biol 8(4):334–338

Bajaj VS, Mak-Jurkauskas ML, Belenky M, Herzfeld J, Griffin RG (2009) Functional and shunt states of bacteriorhodopsin resolved by 250 GHz dynamic nuclear polarization-enhanced solid-state NMR. Proc Natl Acad Sci USA 106(23):9244–9249

Baldus M, Petkova AT, Herzfeld J, Griffin RG (1998) Cross polarization in the tilted frame: assignment and spectral simplification in heteronuclear spin systems. Mol Phys 95(6):1197–1207

Barbet-Massin E, Pell AJ, Retel JS, Andreas LB, Jaudzems K, Franks WT, Nieuwkoop AJ, Hiller M, Higman V, Guerry P, Bertarello A, Knight MJ, Felletti M, Le Marchand T, Kotelovica S, Akopjana I, Tars K, Stoppini M, Bellotti V, Bolognesi M, Ricagno S, Chou JJ, Griffin RG, Oschkinat H, Lesage A, Emsley L, Herrmann T, Pintacuda G (2014) Rapid proton-detected NMR assignment for proteins with fast magic angle spinning. J Am Chem Soc 136(35):12489–12497

Bayrhuber M, Meins T, Habeck M, Becker S, Giller K, Villinger S, Vonrhein C, Griesinger C, Zweckstetter M, Zeth K (2008) Structure of the human voltage-dependent anion channel. Proc Natl Acad Sci USA 105(40):15370–15375

Bennett AE, Rienstra CM, Auger M, Lakshmi KV, Griffin RG (1995) Heteronuclear decoupling in rotating solids. J Chem Phys 103:1–8

Bennett AE, Rienstra C, Griffiths J, Zhen W, Lansbury P, Griffin R (1998) Homonuclear radio frequency-driven recoupling in rotating solids. J Chem Phys 108(22):9463–9479

Bhate MP, McDermott AE (2012) Protonation state of E71 in KcsA and its role for channel collapse and inactivation. Proc Natl Acad Sci USA 109(38):15265–15270

Bhate MP, Wylie BJ, Tian L, Mcdermott AE (2010) Conformational dynamics in the selectivity filter of KcsA in response to potassium ion concentration. J Mol Biol 401:1–12

Brunner JD, Lim NK, Schenck S, Duerst A, Dutzler R (2014) X-ray structure of a calcium-activated TMEM16 lipid scramblase. Nature 516(7530):207–212

Cherezov V, Rosenbaum DM, Hanson MA, Rasmussen SG, Thian FS, Kobilka TS, Choi H-J, Kuhn P, Weis WI, Kobilka BK (2007) High-resolution crystal structure of an engineered human β2-adrenergic G protein-coupled receptor. Science 318(5854):1258–1265

Cross TA, Ekanayake V, Paulino J, Wright A (2014) Solid state NMR: the essential technology for helical membrane protein structural characterization. J Magn Reson 239(C):100–109

Delaglio F, Grzesiek S, Vuister GW, Zhu G, Pfeifer J, Bax A (1995) NMRPipe: a multidimensional spectral processing system based on UNIX pipes. J Biomol NMR 6(3):277–293

Dolder M, Zeth K, Tittmann P, Gross H, Welte W, Wallimann T (1999) Crystallization of the human, mitochondrial voltage-dependent anion-selective channel in the presence of phospholipids. J Struct Biol 127(1):64–71

Doré AS, Robertson N, Errey JC, Ng I, Hollenstein K, Tehan B, Hurrell E, Bennett K, Congreve M, Magnani F, Tate CG, Weir M, Marshall FH (2011) Structure of the adenosine A2A Receptor in complex with ZM241385 and the Xanthines XAC and Caffeine. Structure 19(9):1283–1293

Eddy MT, Yu T-Y (2014) Membranes, peptides, and disease. Unraveling the mechanisms of viral proteins with solid state nuclear magnetic resonance spectroscopy. Solid State Nucl Magn Reson 61–62:1–7

Eddy MT, Ong T-C, Clark L, Teijido O, van der Wel PCA, Garces R, Wagner G, Rostovtseva TK, Griffin RG (2012) Lipid dynamics and protein–lipid interactions in 2D crystals formed with the β-barrel integral membrane protein VDAC1. J Am Chem Soc 134:1–8

Etzkorn M, Martell S, Andronesi OC, Seidel K, Engelhard M, Baldus M (2007) Secondary structure, dynamics, and topology of a seven-helix receptor in native membranes, studied by solid-state NMR spectroscopy. Angew Chem Int Ed 46(3):459–462

Fernández C, Adeishvili K, Wüthrich K (2001) Transverse relaxation-optimized NMR spectroscopy with the outer membrane protein OmpX in dihexanoyl phosphatidylcholine micelles. Proc Natl Acad Sci USA 98(5):2358–2363

Fernández C, Hilty C, Wider G, Güntert P, Wüthrich K (2004) NMR structure of the integral membrane protein OmpX. J Mol Biol 336(5):1211–1221

Frericks HL, Zhou DH, Yap LL, Gennis RB, Rienstra CM (2006) Magic-angle spinning solid-state NMR of a 144 kDa membrane protein complex: E. coli cytochrome bo3 oxidase. J Biomol NMR 36(1):55–71

Goddard TD, Kneller GD SPARKY 3. University of California, San Francisco

Griffiths J, Bennett A, Engelhard M, Siebert F, Raap J, Lugtenburg J, Herzfeld J, Griffin R (2000a) Structural investigation of the active site in bacteriorhodopsin: geometric constraints on the roles of Asp-85 and Asp-212 in the proton-pumping mechanism from solid state NMR. Biochemistry 39(2):362–371

Griffiths JM, Bennett AE, Engelhard M, Siebert F, Raap J, Lugtenburg J, Herzfeld J, Griffin RG (2000b) Structural investigation of the active site of bacteriorhodopsin: geometric constraints on the roles of Asp-85 and Asp-212 in the proton pumping mechanism from solid-state NMR. Biochemistry 39:362–371

Harbison GS, Smith SO, Pardoen JA, Courtin JM, Lugtenburg J, Herzfeld J, Mathies RA, Griffin RG (1985) Solid-state 13C NMR detection of a perturbed 6-s-trans chromophore in bacteriorhodopsin. Biochemistry 24(24):6955–6962

Heise H, Hoyer W, Becker S, Andronesi OC, Riedel D, Baldus M (2005) Molecular-level secondary structure, polymorphism, and dynamics of full-length alpha-synuclein fibrils studied by solid-state NMR. Proc Natl Acad Sci USA 102(44):15871–15876

Higman VA, Flinders J, Hiller M, Jehle S, Markovic S, Fiedler S, Rossum B-J, Oschkinat H (2009) Assigning large proteins in the solid state: a MAS NMR resonance assignment strategy using selectively and extensively 13C-labelled proteins. J Biomol NMR 44(4):245–260

Hiller M, Krabben L, Vinothkumar KR, Castellani F, van Rossum BJ, Kuhlbrandt W, Oschkinat H (2005) Solid-state magic-angle spinning NMR of outer-membrane protein G from *Escherichia coli*. ChemBioChem 6(9):1679–1684

Hiller M, Higman VA, Jehle S, van Rossum B-J, Kühlbrandt W, Oschkinat H (2008a) [2,3-(13)C]-labeling of aromatic residues-getting a head start in the magic-angle-spinning NMR assignment of membrane proteins. J Am Chem Soc 130(2):408–409

Hiller S, Garces RG, Malia TJ, Orekhov VY, Colombini M, Wagner G (2008b) Solution structure of the integral human membrane protein VDAC-1 in detergent micelles. Science (New York, NY) 321(5893):1206–1210

Hiller S, Malia TJ, Garces RG, Orekhov VY, Wagner G (2010) Backbone and ILV side chain methyl group assignments of the integral human membrane protein VDAC-1. Biomol NMR Assign 4(1):29–32

Hing A, Vega S, Schaefer J (1993) Measurement of heteronuclear dipolar coupling by transferred-echo double-resonance NMR. J Magn Reson Ser A 103(2):151–162

Hino T, Arakawa T, Iwanari H, Yurugi-Kobayashi T, Ikeda-Suno C, Nakada-Nakura Y, Kusano-Arai O, Weyand S, Shimamura T, Nomura N, Cameron AD, Kobayashi T, Hamakubo T, Iwata S, Murata T (2012) G-protein-coupled receptor inactivation by an allosteric inverse-agonist antibody. Nature 482(7384):237–240

Hodge T, Colombini M (1997) Regulation of metabolite flux through voltage-gating of VDAC channels. J Membr Biol 157(3):271–279

Hong M, Zhang Y, Hu F (2012) Membrane Protein Structure and Dynamics from NMR Spectroscopy. Annu Rev Phys Chem 63(1):1–24

Hu JG, Sun BQ, Bizounok M, Hatcher ME, Lansing JC, Raap J, Verdegem PJE, Lugtenburg J, Griffin RG, Herzfeld J (1998) Early and late M intermediates in the bacteriorhodopsin photocycle: a solid-state NMR study. Biochemistry 37:8088–8096

Hwang PM, Choy W-Y, Lo EI, Chen L, Forman-Kay JD, Raetz CRH, Privé GG, Bishop RE, Kay LE (2002) Solution structure and dynamics of the outer membrane enzyme PagP by NMR. Proc Natl Acad Sci USA 99(21):13560–13565

Jaroniec C, Filip C, Griffin R (2002a) 3D TEDOR NMR experiments for the simultaneous measurement of multiple carbon-nitrogen distances in uniformly 13C, 15 N-labeled solids. J Am Chem Soc 124(36):10728–10742

Jaroniec CP, Filip C, Griffin RG (2002b) 3D TEDOR NMR experiments for the simultaneous measurement of multiple carbon-nitrogen distances in uniformly (13)C, (15)N-labeled solids. J Am Chem Soc 124(36):10728–10742

Krabben L, van BJ Rossum, Jehle S, Bocharov E, Lyukmanova EN, Schulga AA, Arseniev A, Hucho F, Oschkinat H (2009) Loop 3 of short neurotoxin II is an additional interaction site with membrane-bound nicotinic acetylcholine receptor as detected by solid-state NMR spectroscopy. J Mol Biol 390(4):662–671

Lakshmi KV, Auger M, Raap J, Lugtenburg J, Griffin RG, Herzfeld J (1993) Internuclear distance measurement in a reaction intermediate: solid-state ^{13}C NMR rotational resonance determination of the Schiff-base configuration in the M-photointermediate of bacteriorhodopsin. J Am Chem Soc 115:8515–8516

Lange A, Giller K, Pongs O, Becker S, Baldus M (2006) Two-dimensional solid-state nmr applied to a chimeric potassium channel. J Recept Signal Transduct 26(5–6):379–393

Lansing JC, Hohwy M, Jaroniec CP, Creemers AFL, Lugtenburg J, Herzfeld J, Griffin RG (2002) Chromophore distortions in the bacteriorhodopsin photocycle: evolution of the H-C14-C15-H dihedral angle measured by solid-state NMR. Biochemistry 41(2):431–438

Li Y, Berthold DA, Gennis RB, Rienstra CM (2008) Chemical shift assignment of the transmembrane helices of DsbB, a 20-kDa integral membrane enzyme, by 3D magic-angle spinning NMR spectroscopy. Protein Sci 17(2):199–204

Liang B, Tamm LK (2007) Structure of outer membrane protein G by solution NMR spectroscopy. Proc Natl Acad Sci USA 104(41):16140–16145

Mak-Jurkauskas ML, Bajaj VS, Hornstein MK, Belenky M, Griffin RG, Herzfeld J (2008) Energy transformations early in the bacteriorhodopsin photocycle revealed by DNP-enhanced solid-state NMR. Proc Natl Acad Sci USA 105(3):883–888

Malia TJ, Wagner G (2007) NMR structural investigation of the mitochondrial outer membrane protein VDAC and its interaction with antiapoptotic Bcl-xL. Biochemistry 46(2):514–525

Mannella CA (1997) Minireview: on the structure and gating mechanism of the mitochondrial channel, VDAC. J Bioenerg Biomembr 29(6):525–531

McDermott AE (2004) Structural and dynamic studies of proteins by solid-state NMR spectroscopy: rapid movement forward. Curr Opin Struct Biol 14(5):554–561

McDermott A (2009) Structure and dynamics of membrane proteins by magic angle spinning solid-state NMR. Annu Rev Biophys 38:385–403

Morcombe CR, Gaponenko V, Byrd RA, Zilm KW (2004) Diluting abundant spins by isotope edited radio frequency field assisted diffusion. J Am Chem Soc 126(23):7196–7197

Morris G, Freeman R (1979) Enhancement of nuclear magnetic resonance signals by polarization transfer. J Am Chem Soc 101(3):760–762

Oxenoid K, Chou JJ (2005) The structure of phospholamban pentamer reveals a channel-like architecture in membranes. Proc Natl Acad Sci USA 102(31):10870–10875

Park SH, Das BB, Casagrande F, Tian Y, Nothnagel HJ, Chu M, Kiefer H, Maier K, Angelis AAD, Marassi FM, Opella SJ (2012) Structure of the chemokine receptor CXCR1 in phospholipid bilayers. Nature 491(7426):779–783

Pines A, Gibby M, Waugh J (1973) Proton-enhanced NMR of dilute spins in solids. J Chem Phys 59(2):569–590

Pryor E, Horanyi P, Clark K, Fedoriw N, Connelly S, Koszelak-Rosenblum M, Zhu G, Malkowski M, Wiener M, Dumont M (2013) Structure of the integral membrane protein CAAX protease Ste24p. Science (New York, NY) 339(6127):1600–1604

Reckel S, Gottstein D, Stehle J, Löhr F, Verhoefen MK, Takeda M, Silvers R, Kainosho M, Glaubitz C, Wachtveitl J (2011) Solution NMR structure of proteorhodopsin. Angew Chem Int Ed 50(50):11942–11946

Renault M, Saurel O, Czaplicki J, Demange P, Gervais V, Löhr F, Réat V, Piotto M, Milon A (2009) Solution State NMR structure and dynamics of KpOmpA, a 210 residue transmembrane domain possessing a high potential for immunological applications. J Mol Biol 385(1):117–130

Rosenbaum DM, Cherezov V, Hanson MA, Rasmussen SG, Thian FS, Kobilka TS, Choi H-J, Yao X-J, Weis WI, Stevens RC (2007) GPCR engineering yields high-resolution structural insights into β2-adrenergic receptor function. Science 318(5854):1266–1273

Rostovtseva T, Colombini M (1996) ATP flux is controlled by a voltage-gated channel from the mitochondrial outer membrane. J Biol Chem 271(45):28006–28008

Schein SJ, Colombini M, Finkelstein A (1976) Reconstitution in planar lipid bilayers of a voltage-dependent anion-selective channel obtained from paramecium mitochondria. J Membr Biol 30(2):99–120

Schneider R, Ader C, Lange A, Giller K, Hornig S, Pongs O, Becker S, Baldus M (2008a) Solid-state NMR spectroscopy applied to a chimeric potassium channel in lipid bilayers. J Am Chem Soc 130(23):7427–7435

Schneider R, Ader C, Lange A, Giller K, Hornig S, Pongs O, Becker S, Baldus M (2008b) Solid-state NMR spectroscopy applied to a chimeric potassium channel in lipid bilayers. J Am Chem Soc 130(23):7427–7435

Schneider R, Etzkorn M, Giller K, Daebel V, Eisfeld J, Zweckstetter M, Griesinger C, Becker S, Lange A (2010) The native conformation of the human VDAC1 N terminus. Angew Chem Int Ed Engl 49(10):1882–1885

Schnell JR, Chou JJ (2008) Structure and mechanism of the M2 proton channel of influenza A virus. Nature 451(7178):591–595

Shanmugavadivu B, Apell H-J, Meins T, Zeth K, Kleinschmidt JH (2007) Correct folding of the beta-barrel of the human membrane protein VDAC requires a lipid bilayer. J Mol Biol 368(1):66–78

Shen Y, Delaglio F, Cornilescu G, Bax A (2009) TALOS+: a hybrid method for predicting protein backbone torsion angles from NMR chemical shifts. J Biomol NMR 44(4):213–223

Shi L, Peng X, Ahmed MAM, Edwards D, Brown LS, Ladizhansky V (2008) Resolution enhancement by homonuclear J-decoupling: application to three-dimensional solid-state magic angle spinning NMR spectroscopy. J Biomol NMR 41(1):9–15

Shi L, Ahmed MAM, Zhang W, Whited G, Brown LS, Ladizhansky V (2009a) Three-dimensional solid-state NMR study of a seven-helical integral membrane proton pump-structural insights. J Mol Biol 386(4):1078–1093

Shi L, Lake EMR, Ahmed MAM, Brown LS, Ladizhansky V (2009b) Solid-state NMR study of proteorhodopsin in the lipid environment: secondary structure and dynamics. Biochim Biophys Acta 1788(12):2563–2574

Shi L, Ahmed MAM, Zhang W, Whited G, Brown LS, Ladizhansky V (2009b) Three-dimensional solid-state NMR study of a seven-helical integral membrane proton pump–structural insights-supporting Info. J Mol Biol 1–9

Shimamura T, Shiroishi M, Weyand S, Tsujimoto H, Winter G, Katritch V, Abagyan R, Cherezov V, Liu W, Han GW, Kobayashi T, Stevens RC, Iwata S (2011) Structure of the human histamine H1 receptor complex with doxepin. Nature 475(7354):65–70

Takegoshi K, Nakamura S, Terao T (2001) C-13-H-1 dipolar-assisted rotational resonance in magic-angle spinning NMR. Chem Phys Lett 344(5–6):631–637

Tang M, Sperling LJ, Berthold DA, Schwieters CD, Nesbitt AE, Nieuwkoop AJ, Gennis RB, Rienstra CM (2011) High-resolution membrane protein structure by joint calculations with solid-state NMR and X-ray experimental data. J Biomol NMR 51(3):227–233

Thompson LK, McDermott AE, Raap J, van der Wielen CM, Lugtenburg J, Herzfeld J, Griffin RG (1992) Rotational resonance NMR study of the active site structure in bacteriorhodopsin: conformation of the Schiff base linkage. Biochemistry 31:7931–7938

Thurber KR, Tycko R (2009) Measurement of sample temperatures under magic-angle spinning from the chemical shift and spin-lattice relaxation rate of 79Br in KBr powder. J Magn Reson 196(1):84–87

Ujwal R, Cascio D, Colletier J-P, Faham S, Zhang J, Toro L, Ping P, Abramson J (2008) The crystal structure of mouse VDAC1 at 2.3 A resolution reveals mechanistic insights into metabolite gating. Proc Natl Acad Sci USA 105(46):17742–17747

Varga K, Tian L, McDermott AE (2007) Solid-state NMR study and assignments of the KcsA potassium ion channel of S. lividans. Biochim Biophys Acta 1774(12):1604–1613

Verardi R, Shi L, Traaseth NJ, Walsh N, Veglia G (2011) Structural topology of phospholamban pentamer in lipid bilayers by a hybrid solution and solid-state NMR method. Proc Natl Acad Sci USA 108(22):9101–9106

Wang S, Munro RA, Shi L, Kawamura I, Okitsu T, Wada A, Kim S-Y, Jung K-H, Brown LS, Ladizhansky V (2013) Solid-state NMR spectroscopy structure determination of a lipid-embedded heptahelical membrane protein. Nat Methods 10(10):1007–1012

Williamson PT, Gröbner G, Spooner PJ, Miller KW, Watts A (1998) Probing the agonist binding pocket in the nicotinic acetylcholine receptor: a high-resolution solid-state NMR approach. Biochemistry 37(30):10854–10859

Williamson PT, Verhoeven A, Miller KW, Meier BH, Watts A (2007) The conformation of acetylcholine at its target site in the membrane-embedded nicotinic acetylcholine receptor. Proc Natl Acad Sci USA 104(46):18031–18036

Zhou DH, Nieuwkoop AJ, Berthold DA, Comellas G, Sperling LJ, Tang M, Shah GJ, Brea EJ, Lemkau LR, Rienstra CM (2012) Solid-state NMR analysis of membrane proteins and protein aggregates by proton detected spectroscopy. J Biomol NMR 54(3):291–305